Elastohydrodynamics of Blade Coating

Blade coating is the most common method of coating paper, and it is applied in coating magnetic suspensions and adhesives. Typically, the blade's upstream edge is clamped into a rigid holder so that the blade and substrate form a converging wedge. The translating substrate drags liquid into the wedge, where liquid forces develop and deflect the elastic blade, but it is loaded externally to counteract the deflection. Liquid dragged past the blade and thus the coating thickness depend on the elastohydrodynamic interaction among blade, liquid, and loading. Shell theory and lubrication flow theory describe the interaction by means of differential equations that are shown to be equivalent to Saita and Scriven's (1985) earlier formulation but that lead to a computationally more efficient analysis. Predictions computed agree with those of the earlier formulation and with experiments. Moreover, the new predictions illustrate effects of normal force loading and broaden the theory of blade coating.

F. R. Pranckh
L. E. Scriven
Coating Process Fundamentals Program
Department of Chemical Engineering
& Materials Science
University of Minnesota
Minneapolis, MN 55455

Introduction

Creating a coating requires forming precisely (i.e., 'premetering') the needed liquid sheet and transferring it to the substrate, delivering more liquid than needed and precisely removing the excess (i.e., 'metering the excess off the substrate'), or supplying exactly the amount of liquid carried away by the substrate from a 'pond' whose level is sensed and controlled ('demand feed'). Blade coating is the most prominent approach that relies on flooding the substrate and metering the excess off. It is also used in the demand-feed mode. There are several versions of blade coating.

In knife coating, often encountered in household and laboratory spreading operations, the metering blade is practically rigid (Grant and Satas, 1984). In so-called bevelled-blade, stiff-blade, straight-blade or trailing-blade coating, which is the most common mode of high-speed coating of particulate suspensions in the paper industry, the metering blade in its mounting is significantly deformable (Eklund, 1984). In low-angle-blade, bent-blade or flexible-blade coating, which is encountered too in coating of particulate suspensions, the blade is more or less highly flexed (Gartaganis et al., 1977; Saita and Scriven, 1985). Bent blades are also commonly used to remove excess liquid from the unengraved portions of a knurl or gravure roll (Larkin, 1984; Kistler, 1988) and to smooth the overall uniform, but locally patterned, layers of magnetic suspensions or viscous adhesives that are metered onto a substrate by means of knurl roll or gravure roll.

Whether a blade should be classified as 'stiff' or 'flexible' depends on its elastic properties, in particular its flexural rigidity; the way in which it is mounted; the viscosity of the liquid being coated; and the speed of the substrate past the blade. As Munter (1981) and others as well as Eklund (1984) had observed, and as Saita and Scriven (1985) elucidated from first principles, there is a *continuous* progression from stiff- to flexible-blade behavior in coating operations.

Because in the analysis and experiments of Saita and Scriven (1985) the inertia and impact pressure of the already delivered liquid are negligible, their results do not pertain to high-speed operations like those encountered today in paper coating. Neither does their study account for the effect of blade-tip shape when in the stiff-blade mode it can be significant, nor does it cover the effect of the downstream free surface that separates from the blade tip. On the other hand, their results are benchmarks for any analysis that does incorporate the effects of liquid inertia, blade-tip shape, and downstream free surface. In another paper we report just such a study (Pranckh and Scriven, 1989).

In that study we employ a formulation of the elastic response of a deforming blade different from that of Saita and Scriven (1985). The initial purpose of the present paper is to demonstrate that the two formulations are fully equivalent. The newer formulation leads to a more efficient way of calculating predictions from the governing principles. The second purpose of the present paper is to validate the newer algorithm for calculating predictions and to assess its efficiency. The third purpose it to report some new results that add to the picture of flexible blade coating that Saita and Scriven (1985) put forward.

Blade Coating Action

Coating blades range widely in shape, size, and material, from easily bent plastic strips to far stiffer steel ones. The prototypes here as well as in Saita and Scriven's (1985) study are 0.25- to

0.5-mm-thick, 20- to 100-mm-long steel blades. The blade can be loaded in several ways.

1. Simplest is to pivot it about the clamp to a working angle ϕ_w which is larger than the installation angle ϕ_0 at the clamp when the blade tip first touches the (stationary) substrate.

2. Another way is to press on the blade with an air hose between it and a rigid backing, the air pressure being controllable.

3. The blade also can be pressed with a more or less sharp-edged, spring-loaded or pneumatically-loaded bar, which is arranged in such a way that it delivers a fixed normal force F_N per unit length at a fixed distance s_F along the blade from the clamping axis.

4. Still another method is to press on the blade with a more or less sharp-edged, rigidly-fixed stop, which functions as a secondary pivot axis and to translate the blade clamp so that the blade tip is forced against the substrate as the blade pivots about the stop (Sommer et al., 1987; Nakazawana et al., 1987; Åkesson and Olsson, 1988). Saita and Scriven (1985) studied blades that pivot about the clamping and blades loaded by an air hose that acts on the fraction of the blade from 0.4 to 0.675 of the blade length. Here normal force loading and pivoting about the clamping are studied, the latter for direct comparison to Saita's (1984) predictions and experiments.

The basic action in a blade coater is as follows. The moving substrate, supported by the back-up roll, carries liquid into the wedge formed by the blade and the substrate. If the speed is great enough or the angle large enough there is a significant impact pressure that can be understood in conventional terms of inviscid flow, as Kahila and Eklund (1978) had recognized and we evaluated elsewhere (Pranckh and Scriven, 1988). Here we suppose with Saita and Scriven (1985) that the impact pressure is negligible, so that only the viscous action known as the hydrodynamic lubrication effect is active. Liquid is dragged toward the vertex of the wedge by the moving substrate; and as it does so, the hydrodynamic pressure rises. Thus there is an adverse pressure gradient that induces a pressure-gradient-driven flow component that opposes the viscous-drag-driven flow component. One outcome is that much or most of the liquid is rejected, only a fraction passing into the narrow gap between blade and substrate to become the coated layer. (Note the stagnation line on the blade in Figure 1, which separates the liquid that passes the blade from the rejected liquid.)

A second outcome is that the hydrodynamic pressure and viscous shear stress act on the blade, loading it and deforming it elastically. The elastic deformation induces elastic restoring forces within the blade. These restoring forces, together with any externally applied loading by a pressure hose or a bar, balance the hydrodynamic pressure and viscous shear stress on the blade. The configuration of the deformed blade shapes the flow passage, which in turn influences the flow field and the pressure and viscous stresses in it. These in turn affect the loading of the blade and thus its configuration—the quintessential elastohydrodynamic interaction. The amount of liquid that passes under the blade and is coated can be controlled by the blade stiffness and by the external loading on it.

To analyze the basic action requires solving together the equations that govern the lubrication-type flow in a passage of *a priori* unknown configuration, and the equations governing the elastic response of a shell-type member under *a priori* unknown loading. The latter equations are here formulated differently than those by Saita and Scriven (1985). The lubrication flow equations, however, are the standard Reynolds system and are exactly the same.

Theoretical Principles

Elastic response of the blade

When a coating blade is loaded, the displacements of material locales in the blade can be large; yet their deformations can remain small, because bending effects are prominent and extensional effects remain negligible. The length and width of a coating blade are generally much larger than its thickness. In

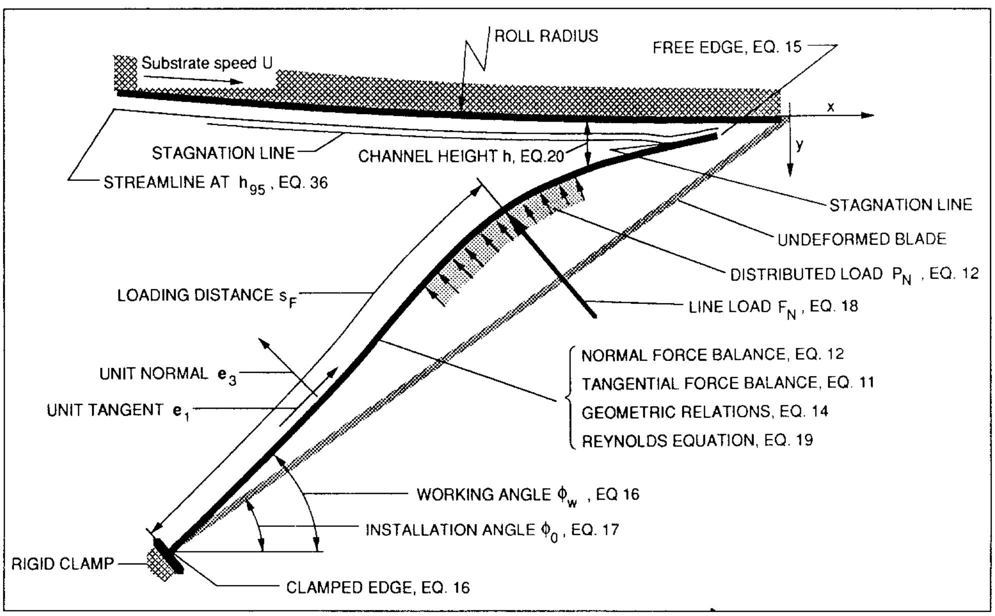

Figure 1. Blade coater as modeled with the governing principles for blade and flow.

addition, if neither loading nor blade material varies across the breadth of the blade, its elastic behavior is described by the theory of inextensible, thin, cylindrical shells. The generators of the cylinders are in the breadthwise direction. The shape of the shell is given by the plane curve in which a plane perpendicular to the generators cuts them. Libai and Simmonds (1988) called such shells beamshells, because their behavior is described by a one-dimensional theory, namely one-dimensional, inextensible, thin, cylindrical shell theory, similar to the nonlinear Euler-Bernoulli beam theory. For beamshells the linear and angular momentum balances for an arbitrary shell control volume are (Green and Zerna, 1968; details of the derivation are recorded by Pranckh, 1989):

$$\boldsymbol{P}(s) + \frac{d}{ds}[\boldsymbol{e}_1(s) \cdot \boldsymbol{T}(s)] = 0, \tag{1}$$

$$\boldsymbol{e}_1(s) \times \boldsymbol{e}_1(s) \cdot \boldsymbol{T}(s) + \frac{d\boldsymbol{M}(s)}{ds} = 0. \tag{2}$$

where $\boldsymbol{P}(s)$ is the vector of the external load (force per unit area) on the shell; $\boldsymbol{T}(s)$, the stress resultant tensor at the shell edges; and $\boldsymbol{M}(s)$, the moment vector at the shell edges; s arc length along the blade. $\{\boldsymbol{e}_1(s), \boldsymbol{e}_2(s), \boldsymbol{e}_3(s)\}$ are the orthonormal basis vectors for the shell indicated in Figure 1: $\boldsymbol{e}_1(s)$ is the tangent along the governing curve, $\boldsymbol{e}_3(s)$ is the normal to the governing curve, and $\boldsymbol{e}_2(s)$ is in the breadthwise direction, $\boldsymbol{e}_2 \equiv \boldsymbol{e}_3 \times \boldsymbol{e}_1$. The stress resultants considered in this theory are the normal shear stress resultant $Q(s)$ and the tangential stress resultant $N(s)$ (Libai and Simmonds, 1988):

$$\boldsymbol{T} \equiv \boldsymbol{e}_1\boldsymbol{e}_1 N + \boldsymbol{e}_1\boldsymbol{e}_3 Q. \tag{3}$$

The moment is around an axis in the breadthwise direction $\boldsymbol{e}_2$. This moment is proportional to the local curvature $C(s)$ according to the simple constitutive relation

$$\boldsymbol{M}(s) \equiv \boldsymbol{e}_2\, M(s) = -\boldsymbol{e}_2\, C(s), \tag{4}$$

where the tangential shear stress resultant N and the normal shear stress resultant Q are measured in units of D/ℓ^2, in which D is the bending stiffness, $D \equiv Et^3/[12(1-\nu^2)]$; E, Young's modulus; t, blade thickness; ν, Poisson's ratio; and ℓ, blade length. The bending moment M is measured in units of D/ℓ; the curvature C, in units of $1/\ell$. With the definition of the stress resultant tensor (Eq. 3) and the constitutive relation (Eq. 4), the linear momentum balance (Eq. 1) can be broken into tangential and normal force balances along the blade, and the moment of momentum balance (Eq. 2) can be reduced to a scalar equation; thus

$$\frac{dN}{ds} - CQ + P_1 = 0, \tag{5}$$

$$\frac{dQ}{ds} + CN + P_3 = 0, \tag{6}$$

$$\frac{dM}{ds} - Q = 0. \tag{7}$$

The constitutive relation (Eq. 4) and the moment of momentum balance (Eq. 7) can be used to eliminate the normal shear resultant $Q(s)$ from the force balances (Eqs. 5 and 6) to yield

$$\frac{dN}{ds} + C\frac{dC}{ds} + P_1 = 0, \tag{8}$$

$$-\frac{d^2C}{ds^2} + CN + P_3 = 0. \tag{9}$$

P_1 and P_3 are the tangential and normal loading, measured in units of D/ℓ^3, which liquid and loading forces exert on the blade. In the lubrication approximation, the liquid tractions depend only on pressure $p(s)$ and channel height $h(s)$,

$$P_1 = -N_{Es}\left(\frac{h}{2}\frac{dp}{ds} - \frac{1}{h}\right) + P_T,$$

$$P_3 = -N_{Es}(-p) + P_N, \tag{10}$$

where h is channel height measured in units of bladeeUlength ℓ; p, pressure in units of $\mu U/\ell$; μ, liquid viscosity; U, substrate speed. The ratio of a characteristic viscous stress, $\mu U/\ell$, to a characteristic elastic stress, D/ℓ^3, is the elasticity number, $N_{Es} \equiv \mu U\ell^2/D$. P_T and P_N are distributed tangential and normal loading forces measured in units of D/ℓ^3. Substituting the liquid tractions and loading (Eq. 10) in the force balances (Eqs. 8 and 9) gives

$$\frac{dN}{ds} + C\frac{dC}{ds}N_{Es}\left(-\frac{h}{2}\frac{dp}{ds} + \frac{1}{h}\right) + P_T = 0, \tag{11}$$

$$-\frac{d^2C}{ds^2} + CN + N_{Es}p + P_N = 0. \tag{12}$$

The coordinates $x(s)$ and $y(s)$ along the blade are related to the blade curvature $C(s)$ and the blade inclination $\beta(s)$ by

$$\frac{d\beta}{ds} = C, \quad \frac{dx}{ds} = \cos\beta, \quad \frac{dy}{ds} = \sin\beta. \tag{13}$$

These three first-order differential equations combine to become the geometric relations between curvature and coordinates:

$$\frac{d^2x}{ds^2} + C\frac{dy}{ds} = 0, \quad \frac{d^2y}{ds^2} - C\frac{dx}{ds} = 0. \tag{14}$$

The boundary conditions on the force and moment balances and geometric relations at the ends of a blade are a free edge and a clamped edge. At the free edge, neither tractions nor moments are exerted on the blade:

$$N = 0, \quad Q = -\frac{dC}{ds} = 0, \quad M = 0. \tag{15}$$

At the clamped edge the position of the clamp and the working angle are prescribed:

$$x = x_M, \quad y = y_M, \quad \frac{dx}{ds} = \cos\phi_w, \quad \frac{dy}{ds} = \sin\phi_w. \tag{16}$$

where x_M and y_M are the location of the clamping measured in units of ℓ; they are calculated from the installation angle ϕ_0 and are not independent parameters:

$$x_M = \cos\phi_0, \quad y_M = -\sin\phi_0. \tag{17}$$

If the blade is loaded with a sharp-edged bar so that the normal force F_N acts on a line across the blade at the distance s_F along the blade from where it is clamped, the normal force adds to the normal shear stress resultant Q, which can be expressed in terms of the curvature gradient (cf. Eqs. 4 and 7),

$$\left.\frac{dC}{ds}\right|_{s_F+} = \left.\frac{dC}{ds}\right|_{s_F-} + N_F, \tag{18}$$

where N_F is the loading number, $N_F \equiv F_N \ell^2/D$.

Lubrication flow of the liquid

If the installation angle of the blade remains less than about 30°, the particle paths in the flow between blade and substrate-wrapped back-up roll are nearly parallel. Along the paths, the rate of change of particle speed is small and so the flow under the blade can be approximated as a lubrication flow (Cameron, 1976). The lubrication approximation to the Navier-Stokes system for incompressible Newtonian liquids reduces to the one-dimensional Reynolds equation, which relates pressure $p(s)$ to channel height $h(s)$ between blade and substrate as a function of arc length s along either:

$$\frac{d}{ds}\left(-\frac{h^3}{12}\frac{dp}{ds} + \frac{h}{2}\right) = 0. \tag{19}$$

The channel height h is measured along rays from the roll center,

$$h = \sqrt{x^2 + (y - R)^2} - R, \tag{20}$$

where R is the radius of the substrate-wrapped back-up roll measured in units of ℓ. The Reynolds equation states that the flow rate q per unit width, measured in units of $U\ell$, is uniform along the channel:

$$q \equiv \left(-\frac{h^3}{12}\frac{dp}{ds} + \frac{h}{2}\right) = \text{constant}. \tag{21}$$

The wet coating thickness h_w, measured in units of ℓ, is in the dimensionless equations equivalent to the flow rate q, $h_w = q$.

The Reynolds equation requires two boundary conditions on pressure. At the inlet side, the pressure boundary condition is an approximation—the flow is approximated as coming from an unbounded pool where the velocity upstream is negligible and the pressure is ambient. At the outlet side, the effect of the downstream free surface that separates from the blade tip is simply neglected and the pressure is taken to be ambient:

$$p = p_a \text{ at } s \rightarrow -\infty, \quad p = p_a \text{ at } s = 1, \tag{22}$$

where p_a is the ambient pressure, which istaken to be zero.

Combined system and parameters

Figure 1 summarizes the combined system of five differential equations, boundary conditions, and auxiliary equations that describes blade coating. The five independent unknown functions of arc length along the blade are the tangential stress resultant N, curvature C, coordinates x and y, and pressure p. Channel height h is a dependent function of the coordinates along the blade and wet coating thickness h_w is a dependent unknown that is evaluated from channel height h and pressure p.

The parameters are the Young modulus, Poisson's ratio, thickness, length, installation angle, and working angle of the blade, the loading distance and loading force for normal force loading, or alternatively hose pressure and blade fraction loaded by the pressure hose for pressure hose loading, the roll radius, substrate speed, and liquid viscosity. Table 1 summarizes the truly physical parameters of blade coating, which are dimensionless numbers: force ratios and geometric ratios that emerge in the derivation of the governing equations.

Relation to integral equations for blade response and liquid flow

For the special case in which the reference point of the moment balance is chosen to be at one crosswise edge of the shell, $s = s_1$, and in which the other crosswise edge is a free edge, in particular the downstream free edge of a coating blade, $s = 1$, the force and moment balances along the blade, Eqs. 5–7, can be expressed with a single integral equation (Pranckh, 1989):

$$\begin{aligned} C(s_1) = -\int_{s_1}^{1} \{&P_3 [\cos\beta(x - x(s_1)) + \sin\beta\,(y - y(s_1))] \\ &+ P_1 [\sin\beta(x - x(s_1)) - \cos\beta\,(y - y(s_1))]\}\, ds. \end{aligned} \tag{23}$$

If the geometric relation between curvature and inclination (Eq. 13a) is invoked, if the expressions for normal and tangential loading (Eq. 10) are substituted, and if the equation is written in dimensional form, then Saita's (1984) version of the moment-of-momentum equation [his Eq. 5.25, which is written in another form as Eq. 1 of Saita and Scriven (1985)] is recovered:

$$\begin{aligned} \left.\frac{d\beta}{ds}\right|_{s_1} = -\frac{1}{D}\int_{s_1}^{\ell} \Big\{ &-(p + P_N)\ [\cos\beta\,(x - x(s_1)) \\ &+ \sin\beta\,(y - y(s_1))] \\ &+ \mu U \left(\frac{h}{2}\frac{dp}{ds} - \frac{1}{h}\right) [\sin\beta\,(x - x(s_1)) \\ &- \cos\beta\,(y - y(s_1))] \Big\}\, ds. \end{aligned} \tag{24}$$

Integrating the Reynolds equation of liquid flow over a length of the flow passage gives

$$p(s_1) = p(0) + 6\mu\, U \int_0^{s_1} \frac{h - K}{h^3}\, ds,$$

$$K \equiv \frac{\left\{\int_0^{\ell} \frac{ds}{h^2} - \frac{p(\ell) - p(0)}{6\mu U}\right\}}{\int_0^{\ell} \frac{ds}{h^3}}. \tag{25}$$

In this form the governing equations for inclination (Eq. 24), coordinates (Eqs. 13b and 13c), and pressure (Eq. 25) require only five boundary conditions, *viz.*, the position and inclination of the blade clamp,

$$x = x_M, \quad y = y_M, \quad \beta = \phi_w \text{ at the clamp,} \tag{26}$$

and the two pressure boundary conditions (Eq. 22). The three boundary conditions (Eq. 15) at the downstream free edge of the blade are already contained in the integral equation (Eq. 24). Saita's four unknown functions of arc length along the blade were the inclination β, coordinates x and y, and pressure p.

Thus the governing principles can be put in two different yet equivalent forms: a set of five differential equations (Eqs. 11, 12, 14 and 19), nine boundary conditions (Eqs. 15, 16 and 22), and an algebraic equation (Eq. 20); or a set of two integral equations (Eqs. 24 and 25a), two differential equations (Eqs. 13b and 13c), five boundary conditions (Eqs. 26 and 22), an algebraic equation that requires quadrature (Eq. 25b), and an algebraic equation (Eq. 20). These two forms differ substantially in the efficiency with which predictions can be calculated from them, as discussed in the next section.

Characteristics of the liquid flow

Once the pressure distribution along the channel is known, the velocity $u(s,z)$, measured in units of substrate speed U, and the shear rate $\dot{\gamma}(s,z)$, measured in units of U/ℓ, can be calculated from the parabolic velocity profile that underlies the Reynolds equation (Eq. 19):

$$u(s, z) = -\frac{1}{2}\frac{dp}{ds}(zh - z^2) + \left(\frac{h - z}{h}\right), \tag{27}$$

$$\dot{\gamma}(s, z) \equiv \frac{du}{dz} = -\frac{1}{2}\frac{dp}{ds}(h - 2z) - \frac{1}{h}, \tag{28}$$

where z is the distance from the substrate measured in units of ℓ.

Local shear is not suitable for comparing the shearing action in a blade coater at different operating conditions. For the purpose of comparison, it is convenient to define the 95th percentile of average shear rate $\bar{\gamma}_{95}(s)$ as the average of the rate of shear suffered by the fastest moving 95% of coated liquid. That is the liquid between the moving substrate and the streamline at a certain height $h_{95}(s)$ that can be calculated from the velocity profile across the channel:

$$0.95q = \int_0^{h_{95}(s)} u(s, z)dz. \tag{29}$$

Thus

$$\bar{\gamma}_{95}(s) \equiv -\frac{1}{h_{95}(s)}\int_0^{h_{95}(s)} \frac{\dot{\gamma}(s, z)}{u(s, z)}dz. \tag{30}$$

Then the 95th percentile of total shear suffered by liquid in the channel is given by

$$\Gamma_{95} \equiv \int_0^1 \bar{\gamma}_{95}(s)\, ds = -\int_0^1 \left[\frac{1}{h_{95}(s)}\int_0^{h_{95}(s)} \frac{\dot{\gamma}(s, z)}{u(s, z)}dz\right] ds. \tag{31}$$

The reason for choosing less than the 100th percentile is now evident: the *total* shear suffered by the liquid passing through the channel is unbounded because liquid in contact with the blade does not flow and so remains indefinitely in the shearing field. Indeed, if there were no pressure gradient, the local velocity profile would be a Couette profile and Eq. 31, rewritten for the fth percentile of total shear, would simplify to

$$\Gamma_f = \frac{1}{h}\left[\frac{1}{1 - \sqrt{1 - f}}\ln\left(\frac{1}{\sqrt{1 - f}}\right)\right].$$

Γ_f depends only on the aspect ratio of the channel, $1/h$, and on f. $\Gamma_{99.9}$ is 3.56 $1/h$, Γ_{99} is 2.56 $1/h$, Γ_{95} is 1.93 $1/h$, and Γ_{90} is 1.68 $1/h$.

If the substrate were porous, liquid under pressure would penetrate the pore space. The pressure-driven uptake by the pore space would be proportional to the permeability of the porous substrate and, in the simplest circumstances, to the integral of the pressure along the channel. Thus for the purpose of comparison it is convenient to define a total pressure force (per unit breadth), P_s (measured in units of μ) that the liquid in the channel exerts on the substrate:

$$P_S \equiv \int_0^1 p(s)ds. \tag{32}$$

Method of Solution

We solved the set of differential equations by representing the unknown functions of distance along the blade, namely N, C, x, y, and p, in terms of linear finite element basis functions on subdomains, or elements, into which we subdivided the blade. The elements were graded towards the blade tip: i.e., we first subdivided the blade starting from the clamp into five segments of blade length, namely 0.4, 0.3, 0.25, 0.025, and 0.025, and then subdivided each segment with a percentage of the total number of elements, namely 15, 23, 39, 8 and 15%. This element grading with 130 element led to solutions that did not change by more than 4% upon doubling the number of elements (cf. the next section). The coefficients of the basis functions were found by solving the algebraic equations for vanishing of the weighted residuals of the differential equations with respect to the same set of linear finite element basis functions (three-point Gauss qaudrature was used for the integration). This is the Galerkin/finite element method (Strang and Fix, 1973).

The resulting set of algebraic equations numbered 700 to 1,500, depending on the number of elements needed to achieve the desired resolution, specifically flow rates that changed less than 4% on further increasing the number and decreasing the size of elements. The set was nonlinear and was solved by Newton iteration.

At each chosen set of parameter values, the Newton iteration was started with an initial estimate that was the solution at a nearby parameter set, i.e., zeroth-order continuation, or that was gotten from a nearby solution by first-order continuation, which required the Jacobian matrix of that solution. The parameter step from that solution was controlled so that the Newton process converged in no more than five iterations. The convergence criterion was that the root-mean-square difference between successive Newton iterates be less than 0.1%. With 1,500 equations, each iteration took about 0.37 second of CPU time on the Cray 2 computer at the University of Minnesota.

The very first set of parameter values was chosen to include a working angle smaller than the installation angle and zero normal force loading on the blade, because then the blade is straight and the pressure is everywhere small. A simple guess of the solution was a straight blade and zero hydrodynamic pressure. That guess fell within the domain of convergence of the Newton process, which could then be continued.

Comparison with integral formulation

The Newton process requires the Jacobian matrix of sensitivities of all the weighted residuals to each coefficient of a finite element basis function. In the differential formulation used here, the Jacobian matrix is sparse and banded, with a block structure that makes a frontal solver an efficient means of solving the linearized equation set at each iteration [a modified version of Hood's (1973) frontal solver was actually used]. A frontal solver requires the order of $n_f^2\, n_p$ computational operations for the Gauss elimination, where n_f is the front width—about 20 in the case of the differential formulation—and n_p is the total number of weighted residual equations.

In contrast, in the integro-differential formulation used by Saita (1984), which for a given division into finite elements leads to the same number of algebraic equations as the differential formulation, the Jacobian matrix is fairly dense below the main diagonal, so dense that a full-matrix solver had to be used. A full-matrix solver requires the order of n_p^3 operations for the Gauss elimination.

In the computer programs for blade coating, the Gauss elimination is the most computationally intensive part, and so the total computer time, and hence the cost of each solution, is roughly proportional to the number of operations required for Gauss elimination. Thus a differential formulation that reduces to 1,000 equations takes the order of 4×10^5 operations to solve, whereas an integro-differential formulation that reduces to the same number of equations takes the order of 10^9 operations. Plainly the differential formulation is much more efficient—2,500 times—and the advantage heightens as n_p, the number of equations, rises, because the ratio of efficiencies is $(n_p/20)^2$.

Results

Sensitivity to normal force loading

As the blade is loaded by an increasing force acting at $s_F = 0.65$, i.e., as the loading number N_F is raised, the coating thickness first falls abruptly to a minimum, rises again, reaches a maximum, and then falls moderately. Figure 2 shows the wet coating thickness h_w vs. the loading number N_F at different elasticity numbers N_{Es}, the latter reflecting the ratio of characteristic viscous to elastic stress. The lower the elasticity number, i.e., the smaller the viscous forces or the greater the blade stiffness, the thinner the coating and the more pronounced the extrema in the operating curve. At elasticity numbers below 10^{-2}, there are coating thicknesses that can be achieved with three different loadings, as Saita and Scriven (1985) pointed out.

An example is instructive. At an elasticity number $N_{Es} = 10^{-3}$ the wet coating thickness h_w of 1.5×10^{-4} can be produced with loading numbers N_F of 1.02, 5.85 or 33.4; all three are marked in Figure 3. With a 40-mm-long, 0.381-mm-thick steel blade at a line speed of 13.33 m/s and a 50-mPa liquid, the wet thickness would be 6 μm, and the three loadings would be 680, 3,900 and 22,300 N/m at 14 mm from the end of the blade.

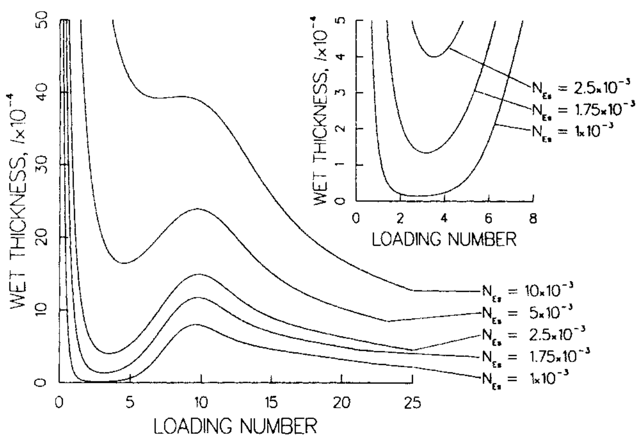

Figure 2. Operating curves under normal loading at different elasticity numbers.
Installation angle, $\phi_0 = 15°$; working angle, $\phi_w = 15°$; distance to loading, $s_F = 0.65$; roll radius, $R = 12.5$.

The extrema in the operating curve mark the boundaries between operating modes. Point 4 in Figure 3 divides the stiff- or bevelled-blade mode to the left from the flexible- or bent-blade mode to the right. The region from the minimum at Point 4 to the inflection in the vicinity of Point 2 is sometimes called the intermediate region, the term bent-blade mode being reserved for the region to the right of the inflection, and 'highly bent blade' for the region to the right of the maximum at Point 5 (cf. Eklund, 1984).

The sequence of the five states labeled in Figure 3 illustrates the underlying physics of blade coating, first explained by Saita and Scriven (1985). As the blade is initially loaded, it is pressed down but deforms little; and the channel between the blade and the substrate narrows to the blade tip, where the hydrodynamic forces concentrate. The coating thickness falls sharply as the blade tip is pressed toward the substrate, reaching a minimum at Point 4, a state in which the pressure peaks extremely sharply at 9×10^5 $[\mu U/\ell]$ very close to the tip, at $s = 0.99995$. Upon

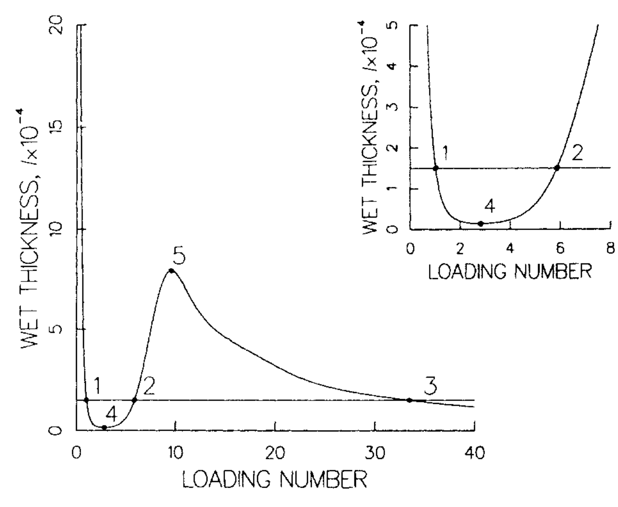

Figure 3. Operating curve under normal loading.
Points 1, 2 and 3 lead to the same coating thickness of 1.5×10^{-4}. Elasticity numbers, $N_{Es} = 10^{-3}$; installation angle, $\phi_0 = 15°$; working angle, $\phi_w = 15°$; distance to loading, $s_F = 0.65$; roll radius, $R = 12.5$.

further loading the hydrodynamic forces begin to bend the blade so that the channel slope decreases at the tip, the pressure peak widens and shifts upstream, the blade tip lifts, and the coating thickness rises, reaching a maximum at Point 5, a state in which the pressure peaks smoothly at 4.35×10^4 $[\mu U/\ell]$ further back from the tip, at $s = 0.95$. At Point 5 the blade is deformed enough that the tip region is parallel to the substrate. Upon further loading the hydrodynamic forces respond so as to bend the blade more and it begins to conform to the substrate-wrapped back-up roll and to form a diverging channel at the tip; the pressure peak broadens and retracts further and the coating thickness falls again. The shifting competition between the loading force, the hydrodynamic pressure and shear forces that develop in response, and elastic forces in the blade that also appear in response, was examined in detail, in terms of force moments, by Saita (1984). This competition was further discussed by Kistler (1988).

Figure 4 shows the theoretical model that predicts distributions of pressure, channel height, curvature, and the blade in each of the three operating states. In Operating State 1, the blade is nearly straight and its curvature is small (although there is a jump in curvature gradient where the loading is applied). Thus the channel converges with nearly constant slope to the blade tip. The pressure rises to a peak value of 4.51×10^4 close to the tip, at $s = 0.9994$. In Operating State 2, the blade is moderately bent. The channel converges with diminishing slope as the tip is approached. The pressure peak is wider, higher at 1.36×10^5, and shifted upstream to $s = 0.998$. In Operating State 3, the blade is substantially deformed. The curvature in the tip region is negative, which indicates that the blade conforms to the substrate-wrapped back-up roll. The channel converges at first and then runs parallel, but diverges at the tip. The pressure peak is still higher at 4.34×10^5 and is shifted way upstream to $s = 0.74$. Moreover, downstream of that place the pressure oscillates, passing through substantially subambient values, and reaches ambient at the tip with a positive gradient. Similar oscillations were predicted for the elastohydrodynamic interaction in a foil bearing by Barlow (1967) and measured experimentally by Licht (1968).

The total pressure that acts on the substrate, P_S from Eq. 32, rises from 570 in the bevelled to 3,180 in the bent mode, and climbs to 27,100 in the highly bent mode. Pressure-driven penetration into the substrate, if porous, would be nearly nine times greater in the highly bent mode than in the bent mode.

The distribution of average shear along the blade reveals further differences in the flow regimes (Figure 5). In the bevelled mode, the streamline at h_{95} runs parallel to the substrate nearly to the blade tip where most of the shear is concentrated. The total shear suffered, Γ_{95} from Eq. 31, is 107. In the bent mode, the shear distributes more evenly, the maximum in average shear shifts upstream, and the total shear suffered mounts to 236. In the highly bent mode, the last quarter of the blade is nearly parallel to the substrate, the average shear rises to a maximum at $s \approx 0.7$, from which it decreases little, and the total shear climbs to 2,110. The stagnation line (a point in cross-sectional views) falls upstream of where the streamline at h_{95} (indicated in Figure 5) first approaches the blade.

Saita and Scriven (1985) linked streaking and scratching defects in coating of shear-thinning suspensions to the region around the stagnation line where shear rates are small and

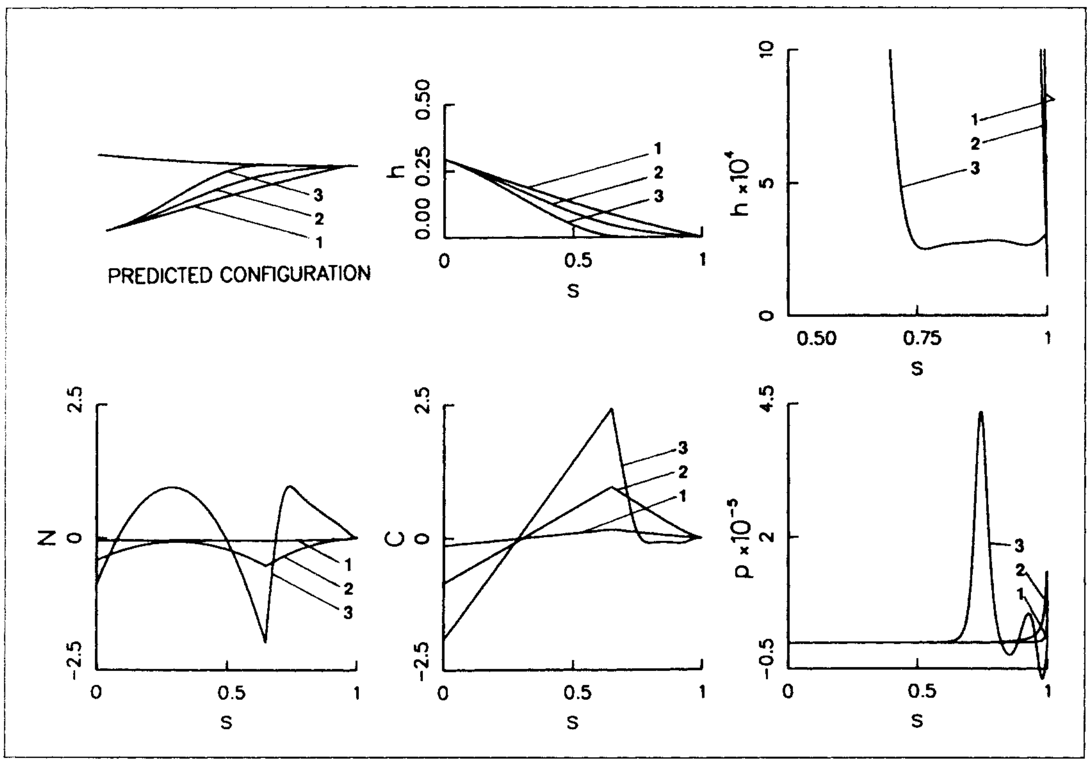

Figure 4. Comparison of three operating points that lead to the same coating thickness.

Coating thickness, $h_w = 1.5 \times 10^{-4}$; elasticity number, $N_{Es} = 10^{-3}$; installation angle, $\phi_0 = 15°$; working angle, $\phi_w = 15°$; distance to loading, $s_F = 0.65$; normal loading, $F_N = 1.02$, 5.85, and 33.4; roll radius, $R = 12.5$.

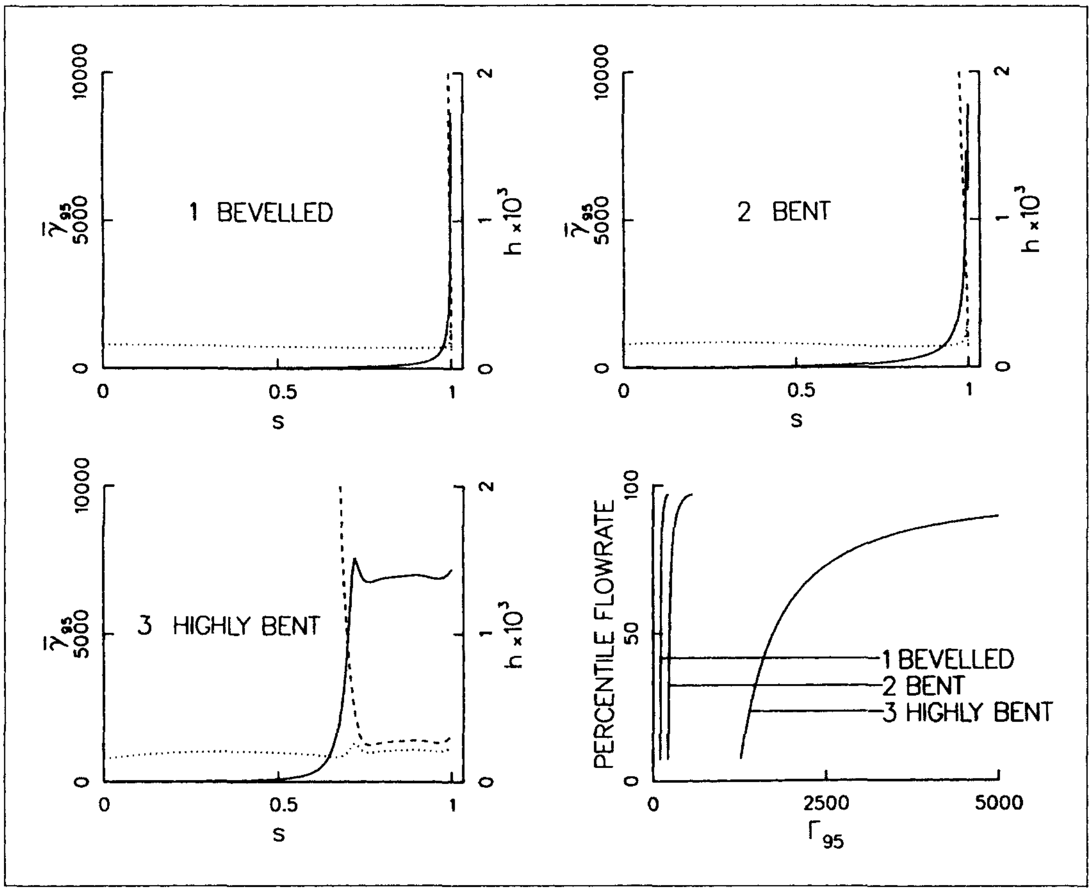

Figure 5. Distribution of shear along the blade and across the coated liquid.
———, average shear suffered $\bar{\gamma}_{95}$ along the blade; · · · · ·, streamline at h_{95}; and ——, channel height.

shear-thinning viscosities are high. Therefore, close to the stagnation line larger particles can get trapped, which leads to streaks, and suspensions can form particle aggregates, which leads to coating defects if aggregates get dislodged and the shear they suffer downstream does not suffice to break them up. Even though the predictions above are for Newtonian liquids, they pertain to streaking and scratching, because shear thinning does not change the basic mechanism of blade coating (Saita and Scriven, 1985).

In the highly bent mode, the stagnation point is at $s \approx 0.7$, and downstream of there the liquid is subject to prolonged shear (Figure 5), which can break up dislodged particle aggregates and which can also be advantageous to orient nonspherical particles such as those used in magnetic recording media. Interestingly, membrane coating, developed in the magnetic media industry (Pipkin, 1984), presents virtually the same distribution of average shear along the flow channel (Pranckh, 1989) and can be designed specifically to subject the liquid to prolonged shear, but avoids the low subambient pressure at the outlet that can lead to cavitation in blade coaters (Eklund, 1984). In the bent mode, the stagnation line is close to the blade tip and downstream of the line the liquid is subjected to some shear, but the high total pressure on the substrate and the low subambient pressure at the outlet are lacking.

In the bevelled mode, the stagnation line is still closer to the blade tip, and downstream of the line the liquid is scarcely sheared at all. This is apparently why the bevelled mode is more susceptible to streaks. Another disadvantage of the bevelled mode is that slight loading variations, which are more difficult to control at low loadings, have significant effects on the coating thickness.

Sensitivity to operating parameters

In Figure 6 is shown the response of the operating states at Point 1 (bevelled mode) and Point 2 (bent mode) in Figure 3 to changes in the operating parameters that cover coating thicknesses from 1 μm to 20 μm for a 40-mm-long, 0.381-mm-thick steel blade at a line speed of 13.33 m/s and a 50-mPa liquid.

As noted above, *increasing the normal force decreases the* coating thickness in the bevelled mode and increases the coating thickness in the bent mode. In both operating states, raising either speed or viscosity (only the product of speed and viscosity, μU, is relevant in the lubrication approximation), reducing blade bending stiffness, and raising blade length all make the coating thicker. In the bent mode, the coating thickness reacts nearly *linearly to the changes of parameter over the range investigated,* whereas in the bevelled mode response diminishes as the coating becomes thinner, because the hydrodynamic pressure concentrates at the blade tip and grows large enough to deflect the blade tip. The sensitivity to any of the four parameters, μ, U, D, and ℓ, is similar, because stronger viscous stresses, $\mu U/\ell$, close to the blade tip deflect the blade more. Blades of smaller bending stiffness deform more under a fixed loading, and so do longer blades. Shifting the blade loading towards the tip lowers the

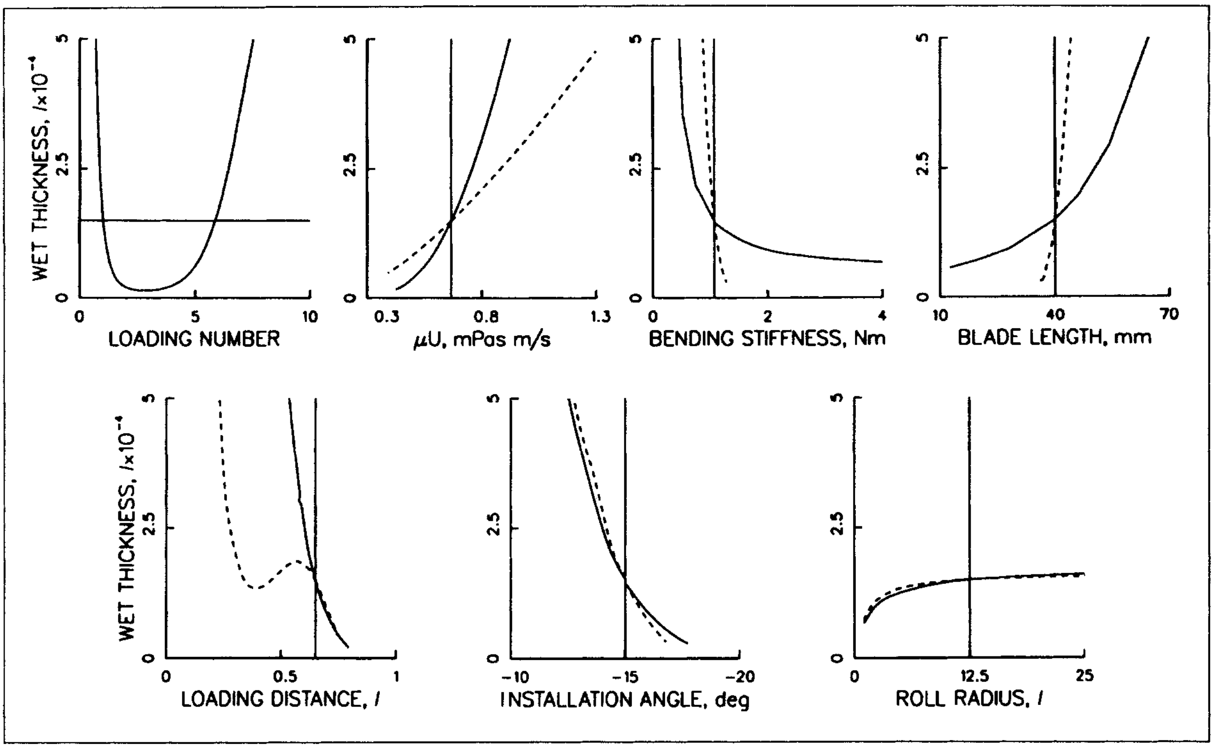

Figure 6. Sensitivity to operating parameters.

———, bevelled mode; — — —, bent mode.

coating thickness in both modes, because the distance between normal force loading and blade tip, where viscous forces concentrate, diminishes. It has the same effect as shortening the blade. At loading distances between 0.55 and 0.4, the blade in bent mode gradually shifts from bent mode behavior to the behavior of a bevelled blade and acts like a bevelled blade at loading distances below 0.4.

If the walls of the wedge formed by blade and substrate were straight (as they nearly are in the bevelled mode), the dependence of the total pressure, P_S from Eq. 32, on the installation angle ϕ_0 could be found from the lubrication approximation (Cameron, 1976),

$$\frac{\partial P_S}{\partial \phi_0} \approx -\frac{6\mu U}{\phi_0^3} \ln\left[\frac{1}{2h_W}(2-\phi_0^2)\right].$$

The total pressure exerted on the blade decreases with increasing installation angle, more so the thinner the coating. Thus, larger installation angles shift the force competition in favor of elastic and external forces and reduce the coating thickness. The sensitivity of the coating thickness to the installation angle is the same for bevelled mode and bent mode—a decrease of the installation angle by merely two degrees more than doubles the coating thickness in both modes.

Decreasing the radius of the substrate-wrapped back-up roll decreases the coating thickness at radii less than two blade lengths, because then the larger roll curvature steepens the wedge between blade and substrate close to the blade tip, which is an effect similar to increasing the installation angle.

Pivoting the blade about the clamp

Pivoting the blade about its clamping, as measured by the working angle ϕ_w induces an external torque at the blade clamp. Elastic restoring forces, which are reaction forces induced by blade deformation, transmit the torque along the blade to the regions of high hydrodynamic pressure and wall shear, which balance the external torque, as the integral moment-of-momentum balance (Eq. 24) nicely shows. Increasing the working angle leads to an operating curve, shown in Figure 7, that is similar to that from increasing the normal force loading. In the bevelled mode, the differences in operating curve and blade configuration between a blade loaded by a normal force and a blade pivoted about the clamp are small, because the blade is nearly straight and thus the moment of the normal force about the clamp is equivalent to the external torque applied at the clamp. But in bent and highly bent modes, blades loaded by an external torque at the clamp deform more in the upstream half as they transmit the torque from the clamp to the regions of high viscous forces downstream. Thus the pivoting mechanism, while effective at low loadings, is not as effective as normal force loading in the bent and highly bent mode.

Quality of the theoretical predictions

The accuracy with which the system of equations can be solved by Galerkin's method with the unknowns approximated by finite element basis functions depends on the order of the basis functions (linear basis functions were used here) and the number of elements into which the domain is divided. An indication of the accuracy was gotten by doubling the number of elements from 130 to 260 (retaining the same distribution of unequal sizes that was chosen to resolve regions of steep

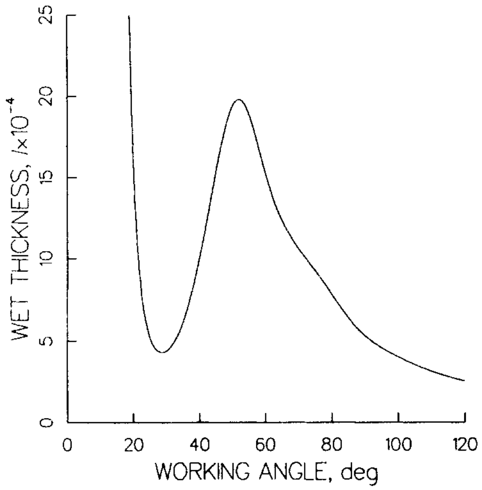

Figure 7. Operating curve as the blade is pivoted about the clamp.
Installation angle, $\phi_0 = 15°$; normal force loading, $F_N = 0$; roll radius, $R = 12.5$.

gradients as well as those of gentle gradients). The quality criterion chosen was the maximum departure of the flow rate in an element from the average of flow rates in all the elements. The ratio of the maximum departure to the average itself was used to construct the bands of uncertainty shown in Figure 8. Doubling the number of elements did not significantly change the predictions of flow rate. At loading numbers greater than 15, the predictions of flow rate with 130 elements were lower, the maximum difference being 4% at a loading number of 22. The insensitivity of theoretical predictions to the doubling of the number of elements indicates that the chosen quality criterion is a highly conservative one. A further indication is the agreement between the predictions and some experiments.

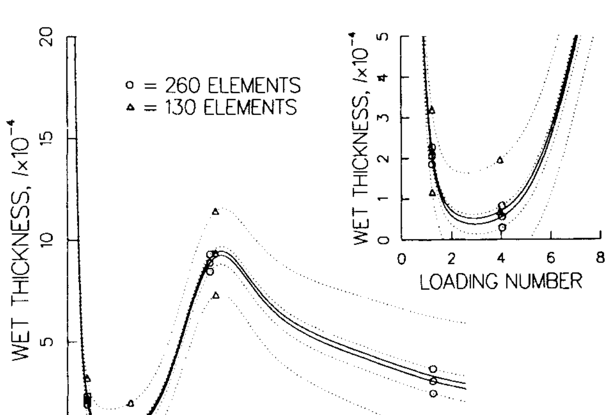

Figure 8. Predictions of the flow rate and the uncertainty of predictions with 130 and 260 unequally spaced elements.
———, predicted flow rate; — — —, uncertainty of predictions. Elasticity number, $N_{Es} = 1.25 \times 10^{-3}$; installation angle, $\theta_0 = 15°$; working angle, $\theta_w = 15°$; loading distance, $s_F = 0.65$; and roll radius, $R = 12.5$.

Table 1. Dimensionless Parameters of Experimental Runs That Govern Blade Coating

Dimensionless Parameter	Definition	Value	Unit
Installation Angle, ϕ_0		24.3	deg
Working Angle, ϕ_w		20–150	deg
Roll Radius, R		1.65	
Loading Distance, S_F		—	
Elasticity Number, N_{Es}	$\frac{\mu U l^2}{D}$	a) $2.59 \cdot 10^{-3}$ b) $3.24 \cdot 10^{-3}$	$\frac{\mu U l^2}{D}$
Loading Number, N_F	$\frac{F_N l^2}{D}$	0	$\frac{F_N l^2}{D}$

Comparison with Saita's Experiments

To validate the differential formulation of the principles of blade coating, which theoretically agrees with Saita and Scriven's (1985) integral formulation, predictions were calculated at the parameters of two experimental runs that Saita (1984) carried out. Predictions were compared not only with his experimental measurements but also with his theoretical predictions from the integral formulation (Table 1 and Figure 9).

In the bevelled mode, the differential formulation predicts up to 50% thinner thicknesses than the ones measured and predicted by Saita. There are two likely causes of the discrepancy. First, the flow in the channel formed by blade tip and substrate, which is not considered in the analysis, can influence the pressure distribution upstream. Second, in the bevelled mode, pressure and viscous forces concentrate at the blade tip; and if the finite element tessellation is not fine enough to resolve the steep gradients, the predicted coating thicknesses are too high. Saita used fewer than 40 handspaced elements along the blade as compared to 260 graded elements used here.

In the bent mode, both theoretical formulations and experiments all agree. In the highly bent mode, especially at elasticity number $N_{Es} = 3.24 \times 10^{-3}$, the differential formulation matches experiments more closely than the integral formulation. The most likely reason is that in the integral formulation,

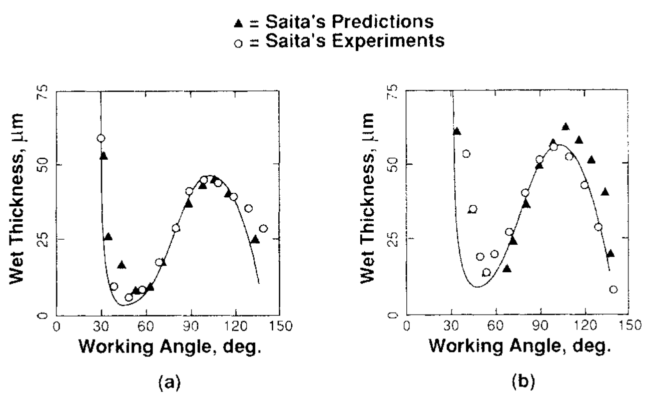

Figure 9. Comparison between this theory and Saita's (1984) theory and experiments.
(a) Elasticity number, $N_{Es} = 2.59 \times 10^{-3}$; installation angle, $\phi_0 = 24.3°$; roll radius, $R = 1.65$.
(b) Elasticity number, $N_{Es} = 3.237 \times 10^{-3}$; installation angle, $\phi_0 = 24.3°$; roll radius, $R = 1.65$.

Saita neglected wall shear stress as a loading on the blade, whereas that stress is significant as shown in the distribution of the tangential stress resultant N in Figure 4.

Summary

The agreement between theoretical predictions and limited experiments validates the elastohydrodynamic theory of blade coating. The differential and integral formulations of the underlying principles considered here—thin cylindrical shell theory and lubrication flow theory—are fully equivalent. However, the differential formulation leads to much more efficient computations. The computed predictions reported here provide new details of the picture of blade coating (cf. Figures 4, 5 and 6). For blades loaded by a normal force, they elucidate the responses of the coating thickness to changes in the operating conditions. Most pronounced are the responses to changes in loading force and installation angle. Moreover, computed predictions reveal the extent of shearing action suffered by the liquid in the distinct operating modes of coating blades.

Stability of blade coating to small disturbances and related secondary flows, associated with ribbing and blade tip wetting downstream and recirculating breadthwise eddies upstream, have not yet been investigated. High-speed blade coating, in which liquid inertia, blade tip shape, and the free surfaces can all be important, was analyzed elsewhere (Pranckh and Scriven, 1988).

Acknowledgment

Discussions with F. A. Saita and the other members of the Coating Flows Research Group at the University of Minnesota were a stimulus for this work. The research was supported in part by a grant-in-aid from the Westvaco Corporation. Computations were made possible by a grant from the Minnesota Supercomputer Institute.

Notation

$\boldsymbol{a}$ = reference point for the moments
$C(s)$ = blade curvature
D = blade bending stiffness
E = blade Young's modules
$e_i(s)$ = orthonormal basis vectors
e_x, e_y = Cartesian basis vectors
F_N = normal loading force
$h(s)$ = channel height
h_w = wet coating thickness
$h_{95}(s)$ = height of streamline that contains 95% of the coated liquid
K = constant of the integral Reynolds equation
l = blade length
$\boldsymbol{M}(s)$ = moment vector
$M(s)$ = bending moment
N_{Es} = elasticity number
N_F = loading number
$N(s)$ = tangential stress resultant
n_f = front width
n_p = total number of weighted residual equations
P_N = external normal loading forces
P_T = external tangential loading forces
P_S = total pressure on the blade or the substrate
P_1 = tangential loading
P_3 = normal loading
p_a = ambient pressure
$p(s)$ = hydrodynamic pressure
$Q(s)$ = normal shear stress resultant
q = flow rate per unit width
$\boldsymbol{r}(s)$ = position vector along the blade
$\boldsymbol{R}(s)$ = moment arm about $\boldsymbol{a}$
R = radius of the substrate wrapped back-up roll
s = arc length along the blade
s_F = loading distance
$T(s)$ = stress resultant tensor
t = blade thickness
U = substrate speed
$u(s,z)$ = liquid velocity
$x(s)$ = blade x-coordinate
x_M = x-location of the clamping
$y(s)$ = blade y-coordinate
y_M = y-location of the clamping
z = distance from the substrate

Greek letters

$\beta(s)$ = blade inclination
$\dot{\underline{\gamma}}(s,z)$ = shear rate
$\gamma_{95}(s)$ = average of the rate of shear suffered
Γ_{95} = 95th percentile of total shear suffered
μ = liquid viscosity
ν = Poisson's ratio
ϕ_0 = blade installation angle
ϕ_w = blade working angle

Literature Cited

Åkesson, R., and A. Olsson, "Neue Billiblade-Konstruktion Verbesserter Qualität und Runnability," *Wochenblatt f. Papierfabrikation,* **8,** 352 (1988).
Barlow, E. J., "Derivation of the Governing Equations for Self-Acting Foil Bearings," *J. Lubric. Theory,* **89,** 6 (1967).
Cameron, A., *Basic Lubrication Theory,* Wiley, New York (1976).
Eklund, D. E., "Influence of Blade Geometry and Blade Pressure on the Appearance of a Coated Surface," *Coating Conf. Proc.,* TAPPI Press, Atlanta (1984).
Gartaganis, P. A., A. J. Cleland, and T. Wairegi, "Blade Mechanics of Extended Blade Coaters," *TAPPI J.,* **64,** 77 (1978).
Grant, O. W., and D. Satas, "Other Knife and Roll Coaters," *Web Processing and Converting Technology and Equipment,* D. Satas, ed., Van Nostrant Rheinbold Co., New York (1984).
Green, A. E., and W. Zerna, *Theoretical Elasticity,* 2nd ed., Oxford University Press, Glasgow (1968).
Hood, P., "Frontal Solution Program for Unsymmetric Matrices," *Int. J. Num. Meth. Eng.,* **10,** 379 (1979).
Kahila, S. J., and D. E. Eklund, "Factors Influencing the Coat Weight in Blade Coating with Bevelled Blades; Theory and Practice," *Coating Conf. Proc.,* TAPPI Press, Atlanta (1978).
Kistler, S. F., "Flexible Blade Doctering in Gravure Coating," *AIChE Meeting,* paper 3B, New Orleans, LA (1988).
Kreyzig, E., *Advanced Engineering Mathematics,* 4th ed., Wiley, New York (1978).
Larkin, M. J., "Gravure coaters," *Web Processing and Converting Technology and Equipment,* D. Satas, ed., Van Nostrant Rheinbold Co., New York (1984).
Libai, A., and J. G. Simmonds, *The Nonlinear Theory of Elastic Shells,* Academic Press, San Diego (1988).
Licht, L., "An Experimental Study: an Elastohydrodynamic Lubrication of Foil Bearings," *J. Lubric. Theory,* **90,** 1 (1968).
Munter, J. D., *personal communications* (1981).
Nakazawana, T., H. Morita, and G. L. Booth, "The Vari-Dwell-Time Blade Coater," *Coating Conf. Proc.,* TAPPI Press, Atlanta (1987).
Pipkin, D. J., "Method of Forming a Coating on a Substrate," *U.S. Patent No. 4,442,144* (1984).
Pranckh, F. R., "Elastohydrodynamics in Coating Flows," *PhD Thesis,* Univ. Minnesota, Minneapolis (1989).
Pranckh, F. R., and L. E. Scriven, "The Physics of Blade Coating of a Deformable Substrate," *Coating Conf. Proc.,* TAPPI Press, Atlanta (1988).
Saita, F. A., "Elastohydrodynamics and Flexible Blade Coating," *PhD Thesis,* Univ. Minnesota, Minneapolis (1984).
Saita, F. A., and L. E. Scriven, "Coating Flow Analysis and the Physics of Flexible Blade Coating," *Coating Conf. Proc.,* TAPPI Press, Atlanta (1985).
Sommer, H., "Influence of Metering Element Geometry on Coat Quality," *Coating Conf. Proc.,* TAPPI Press, Atlanta (1985).
Strang, G., and G. J. Fix, *An Analysis of the Finite Element Method,* Prentice-Hall, Englewood Cliffs, NJ (1973).

Manuscript received May 26, 1989, and revision received Jan. 29, 1990.